공학석사 학위논문

인간 운동 적응의 인코딩 용량에 관하여

On the Encoding Capacity of Human Motor Adaptation

2019년 2월

서울대학교 대학원

기계항공공학부

김 승 연

ABSTRACT

On the Encoding Capacity of Human Motor Adaptation

by

Seungyeon Kim

Department of Mechanical and Aerospace Engineering
Seoul National University

Adaptation of human dynamics to variable environments is well-explained with the concept of the internal model. The internal model is generally parametrized by a combination of motor primitives inspired from the motor cortex neurons. A variety of representations for motor primitives exists, and each model has succeeded in describing certain characteristics of dynamics adaptation. However, the limitations of adaptation explained via the internal model or motor primitives has not been thoroughly addressed in the literature. In particular, the fundamental question of how internal model learning behaves in the presence of signal-dependent noise has yet to be addressed. In this thesis, we try to verify the following hypothesis: "the

larger the encoding space, the better the learning." At the position error level, we investigate how the amount of training and signal-dependent noise interact to adjust the complexity of the force field. To experimentally validate our hypothesis, we perform a set of catch trials for continuous circular motions and quantitatively measure the force field estimated by a human's internal model during the motion. The above two experimental results provide evidence in support of our proposed hypothesis. A simulation study based on a combination of motor primitives is also proposed to verify the experimental results and hypotheses.

Keywords: human motor control, dynamics adaptation, internal model, state-space representation, motor primitives, signal-dependent noise, encoding space

Student Number: 2017-22513

Contents

List of Figures

1

Introduction

When swimming in the water or playing tennis with a tennis racket, humans are subject to a different set of dynamics than what they are normally accustomed to. Additional compensatory forces and torques calculated from models and measurements are required to compensate for the external dynamics in the case of robots, but people can quickly adapt to dynamics in a natural, seemingly effortless fashion. Numerous human motor control studies investigating the human ability to adapt to different arbitrary environments have been presented in the literature, and a number of mathematical models have described the phenomenon that occurs when people adapt to a new set of dynamics. One of these models is the state space internal model framework. The internal model is a dynamic model that can compensate for an external force field, and generalizes to other untrained tasks. The internal model is known to be able to learn only the state-dependent force field; it does not learn any time-varying force fields, even those that are periodic with constant period [1]. Although a time-varying force field cannot be completely

learned with this model, it can be learned through alternative state representations [2, 3]. The acceleration-dependent force field also can be represented by the internal model [4].

Since the internal model is a continuous mapping from state space to muscle force or external force in task space, it is difficult to learn this mapping directly. It is therefore thought to be parametrized for quick and efficient learning, most commonly in the form of motor primitives defined in state space. Specifically, the internal model is parameterized as a linear combination of the motor primitives, with adaptation achieved by adjusting the weights of the primitives [5]. However, no consensus has emerged as to the precise form and definition of the primitives. The most intuitive and basic motor primitive structure is defined as a Gaussian-like function isotropically distributed in state space [5]. These primitives have been revealed to have a bimodal structure, implying that an adaptation would be influenced by the opposing movement [6]. The above primitives are defined above the desired movement state, i.e. the desired state space. However, some researchers argue that learning is not based on the desired state space but on the actual state space. In this context, the primitive of internal model is also studied whether the defined state space is plan-referenced or motion-referenced [7]. Other studies suggest that the internal model is related to position and velocity gains. Some studies have suggested viscoelastic primitive models in which the output of the internal model is position and velocity gain [8]. Other studies suggest that the primitives are encoded as gain fields [9, 10, 11, 12, 13], while other studies suggest that primitives are defined in the error space [14, 15].

However, regardless of the shape, domain, or outputs of the motor primitives, all internal models intrinsically possess a limitation of expressiveness [5, 16]. Perfectly learnable force fields are confined to a subspace that can be expressed by a

fixed set of primitives; otherwise, the internal model only can learn the force field approximately in general. Thus, the internal model cannot fully compensate for a force field in most cases even if the number of learning trials and learning times are sufficient for the adaptation to reach steady state. The difficulty of learning a motor skill differs from motion to motion, especially depending on how much the internal model fits the skill. The difficulty of learning motor skills has been studied by some papers: reaching movements of untrained directions turn out to be even less accurate than before learning [5]; linearity in the position term of the gain field encoding raises the difficulty of learning a force field that is nonlinear with respect to position [9]; correlations in the temporal structure of the adaptation may potentially suggest the easiest and hardest reaching movements to learn [11]. To the best of our knowledge, only a few studies have investigated the degree of learning motor skills at the fully learned phase.

From the perspective of the internal model or motor primitives defined in the velocity space, we hypothesized that if the velocity is fast, it learns well the internal model for the same position trajectory since faster motions will activate more primitives. The related phenomena can be easily found in everyday life. For example, when writing a letter by hand, slow motions often produce more crooked and irregular letters than those written at higher speeds. However, increasing the movement speed also increases the level of noise at the muscle actuators. The multiplicative nature of noise whose variance is linear in the size of the control signal has been verified experimentally in human motor control studies [17, 18]. The effects of the internal model and the multiplicative noise exist simultaneously in the motor learning process, and both concepts have opposite effects on motion error in a single trial. It seems meanginful to further explore the trade-offs between encoding errors and multiplicative noise, but so far no prior research has been conducted

on this topic.

Toward this end, we introduce a new concept called the encoding capacity, which describes how much force field information the internal model can hold. If only the internal model is considered, the encoding capacity can be intuitively defined as the volume of the encoding space. In this paper, we have experimentally shown that the larger the encoding space or encoding capacity, the more effectively a force field can be learned. To extend the encoding space in the state space, we fix the trajectory in the position space and increased the movement speed. As the desired movement speed increases, the motor input becomes larger and therefore receives a larger noise due to the signal-dependent noise. We verified the proposed hypothesis by interpreting the position error-based learning curve according to the complexity of the force field in terms of interaction between encoding capacity and signal-dependent noise. We further develop a channel trial for continuous circular motion, which was not used previously, and use it as a catch trial. We quantitatively determine the extent of learning by estimating the force field that was directly learned by humans while performing the circular motion. Simulation results based on the computational model, particularly the combination of motor primitives, show that the model explains the observed experimental results reasonably well.

The remainder of this thesis is organized as follows. Chapter 2 contains the review and major flow of the human motor control literature. We also introduce the robotic manipulandum "vBOT" which is widely used in human motor control field and used in this thesis. Chapter 3 describes the experiment results that became the motivation for this study. The hypotheses and contributions to be tested in the study are explained. Chapter 4 presents the experimental design and experimental results analysis to verify our main hypothesis. An appropriate simulation

study to explain the experimental results is also proposed. Chapter 5 explains the specific experimental method used in this thesis. Especially, our newly developed catch trial methodology is introduced. Chapter 6 concludes the thesis with summary, some remarks, and future research directions.

2

Human Motor Control Preliminaries

In this chapter, we focus on the background concepts that are required to understand our study. First, we briefly review several existing computational models of motor control. Secondly, we focus on the models that explain human motor adaptation, especially from the perspective of internal models based on the state-space motor primitive and the suggested encoding mechanism. Lastly, we introduce the experimental apparatus, a two-dimensional robotic manipulandum called vBOT, that will be used throughout the study.

2.1 Basic features of human movement

Although different motions are generated when experimenting with different humans, there are some common features in these motions. Features of human motion have been analyzed in various literature, and some of the most prominent features are introduced. These features are also used as an indicator of whether the computation model is convincing in human motor control.

2.1.1 Smooth bell-shaped velocity profile

The most basic task used to analyze human movement in human motor control is the point-to-point reaching movement. When performing reaching movement in the horizontal plane, it is well known that people's hand speeds have a single-peaked bell shaped speed profile. In this case, the position trajectory of the hand usually has the shape of a straight line. Smoothness and graduality of the hand speed profile are found not only in the simple reaching movement but also in various environments, such as when there is an obstacle via point in the middle.

2.1.2 Fitts' law

Fitts' proposed the relation between the task difficulty and movement duration when performing reaching task [19]. Fitts' law is the exact relation expressed in following equation:

$$t = a + b \log_2 \left(\frac{2d}{W} \right) \tag{2.1.1}$$

where a and b are the regression coefficients, t is the movement duration, d is the distance between start and goal target, and W is the goal target width implying accuracy. In Equation 2.1.1, the term $\log \left(\frac{2d}{W} \right)$ means the difficulty of the reaching tasks. This equation is qualitatively a formula to explain the trade-off between speed and task accuracy or variation.

2.1.3 Two-thirds power law

Lacquaniti proposed the relation between the curvature of a human hand path and the corresponding velocity. [20]. This relation is widely referred as the two-thirds power law, and the exact mathematical description of the relation is expressed in

following equation:

$$\omega = c\kappa^{\frac{2}{3}} \tag{2.1.2}$$

where c is a constant, ω is the angular velocity of the hand, and κ is the curvature of the position trajectory path. We can see that velocity and curvature of the trajectory have the nonlinear relationship during the movement in Equation 2.1.2. The above law is a result observed in human hand movement, but it is actually observed also in locomotion or eye-tracking.

2.2 Computational model for human motor control

One of the general paradigm for explaining human motor control is optimal control framework. When humans perform simple point-to-point reaching movements, you can create numerous position trajectory shapes or speed profiles through redundancy of the arms. However, humans create the general motion with common features seen above. In this context, optimal control theory is believed to be one solution to this phenomenon.

2.2.1 Optimization criterion on motor planning

There are researchers who claim that when a task is given, human produces a muscle input that optimizes certain set of objective functions. Optimality not only reproduce the observed behavior but also explain to some extent why a person is generating this motion. There are a variety of candidates as objective functions for describing human movements, but the most widely known and noted functions are introduced in this section.

The most representative objective function is the minimum jerk model proposed by Hogan [21]. This model mainly comes from the smoothness of the hand

trajectory while jerk is the derivation of the hand acceleration. The objective function of the minimum jerk model is proposed by following equation:

$$J = \frac{1}{2}\int_0^{t_f} \left(\frac{d^3x}{dt^3}\right)^2 + \left(\frac{d^3y}{dt^3}\right)^2 dt \tag{2.2.3}$$

where x and y is the Cartesian coordinates of the hand position at time t and t_f is the movement duration. In the special case, we can find a closed trajectory (x, y) that optimizes the objective function in point-to-point movement. For the initial position (x_0, y_0) at time $t = 0$ and goal position (x_f, y_f) at time $t = t_f$, the optimal trajectory is of the following:

$$x(t) = x_0 + (x_f - x_0)\left(10\left(\frac{t}{t_f}\right)^3 - 15\left(\frac{t}{t_f}\right)^4 + 6\left(\frac{t}{t_f}\right)^5\right) \tag{2.2.4}$$

$$y(t) = y_0 + (y_f - y_0)\left(10\left(\frac{t}{t_f}\right)^3 - 15\left(\frac{t}{t_f}\right)^4 + 6\left(\frac{t}{t_f}\right)^5\right) \tag{2.2.5}$$

We assumed that the velocity and acceleration are zero at the start and end of the movement. We can easily check that the position trajectory is straight line and velocity profile is smooth bell-shaped. The minimum-jerk model is a simple and intuitive computation model, but purely based on kinematic parameters of hand position and information about human musculoskeletal system dynamics is not considered when generating motion.

Uno et al. proposed an alternative computation model named the minimum torque-change model [22]. It is a model considering human dynamic parameters unlike the minimum-jerk model, and the objective function of the minimum torque-change model is proposed by following equation:

$$J = \frac{1}{2}\int_0^{t_f} ||\dot{\tau}||^2 dt \tag{2.2.6}$$

where τ is the joint torque input vector of the human arm and $\dot{\tau}$ is the derivation of τ. The minimum-jerk model and the minimum torque-change model appear to be completely different, but the implications are similar because the joint torque and joint acceleration have linear relation locally in the dynamics equation. The minimum jerk model could not reproduce the curvature characteristics of the hand's position trajectory, but the minimum torque-change model is possible. This is because the latter is considering arm dynamics.

2.2.2 Signal-dependent noise : the minimum variance theory

While the above models (i.e. the minimum jerk model or the minimum torque-change model) can account for many aspects of human movement, unexplained features still exist. A simple counterexample is that the above models can be used in situations where the movement duration is precisely given, but in reality people are not. First of all, there is a lack of explanation for the trajectory variance of human movement (i.e. Fitts' law). In this context, Harris et al. proposed a new computational model named the minimum variance model [17]. This model begins with the assumption that human has a positive correlation with the noise variance of the control signal and the absolute value of the control signal. This assumption is generally referred as the signal-dependent noise. In this context, the object of the model is to minimize the variance of the final position in the presence of signal-dependent noise. The objective function of the minimum variance model is proposed by following equation:

$$J = \sum_{t=T+1}^{T+R} \text{trace}(\text{Cov}[x_t]) \tag{2.2.7}$$

where x_t is the state of the hand (i.e. Cartesian position) at time t, T is the time step when human's hand reaches the goal position (i.e. movement duration), and

R is the steps when human maintains hand at the fixed goal position. Through the minimum-variance model, we can explain the characteristics of natural saccadic eye movement and arm movement in reaching movement. Specifically, this model can account for Fitts' law which means observed speed-accuracy trade-off. In conclusion, humans have signal-dependent noise and consider it when motor planning.

2.2.3 Optimal feedback control in motor coordination

As can be seen in the above section, most of the optimality models generate feedforward controllers, or time-dependent policies. In other words, the feedback controller term is not considered. However, given the fact that humans have a complicated structure and noise of arm and motor cortex inputs, and they perform high-level tasks successfully, it's hard to say that a person has only a feedforward controller. So it is believed that feedforward controllers can only have suboptimal performance, and optimal performance is possible when there is a feedback controller. In recent years, the human motor computational model tends to focus on feedback term rather than feedforward term. In this context, the optimal feedback control framework has emerged as a tool to explain the computation model. Todorov proposes an alternative theory based on stochastic optimal feedback control, and show that this strategy allows variability in redundant dimensions of tasks [23]. It has also surprisingly been found that the optimal feedback controller of the human motor system follows the minimum intervention principle [24]. In [23], they assume that the dynamics of human including signal-dependent noise is linear dynamics for numerical simulation. The described simulations have the

following general Linear-Quadratic-Gaussian (LQG) system.

$$\min_{u_0,\cdots u_{T-1}} E\left[\sum_{t=0}^{T} {x_t}^T Q_t x_t + {u_t}^T R u_t\right] \tag{2.2.8a}$$

$$x_{t+1} = Ax_t + Bu_t + \sum_{i=1}^{k} C_i u_t \epsilon_{i,t} \tag{2.2.8b}$$

$$y_t = Hx_t + \omega_t \tag{2.2.8c}$$

Equation 2.2.8's a means the objective function, b means the linear dynamics system of human's hand, and c means the feedback or observation term. $\epsilon_{i,t}$ and ω_t are independent standard normal random variables and independent multivariate normal random variables, respectively, and other parameters are given. When the system noise of dynamics is additive, the solution is well-known. However, we can see that the dynamics, it is confirmed that the signal-dependent noise(or multiplicative noise), not additive noise is reflected in the dynamics. In the case of multiplicative noise, they derived an iterative algorithm for solving this problem. The summarized solution is as following:

$$\hat{x}_{t+1} = A\hat{x}_t + Bu_t + K_t(y_t - H\hat{x}_t) \tag{2.2.9a}$$

$$u_t = -L_t\hat{x}_t \tag{2.2.9b}$$

where K_t is the modified Kalman filter which account for the multiplicative noise, and L_t is the corresponding control law. This new model is able to explain more features as well as basic features such as bell-shaped speed profile. If someone want to apply the optimal feedback control law for the human arm more realistically, you can use the iterative Linear-Quadratic-Gaussian(iLQG) algorithm, which can be applied to nonlinear dynamics.

2.3 Human motor adaptation

The above optimal control views are computational models assuming that people are fully aware of kinematics or dynamics. However, it is difficult to assume that people know this information correctly. The kinematic and dynamic parameters of humans change as they grow, and the external dynamics environment is not constant (i.e. swimming in the water). In the case of the optimal feedback control view, suppose that parameters A and B are unknown or additional nonlinear term $f_e(x, u)$ is added in the dynamics. Therefore, humans are believed to be doing dynamics adaptation separately or simultaneously from optimal control, and there are numerous studies related to motor learning and dynamics adaptation.

2.3.1 Internal model : state representation of motor learning

Consider the dynamic equation in the human arm. The dynamics of the arm expressed by a nonlinear differential equation that relates the vector of joint angles q, the vector of joint angular velocities $\dot{q}$, and the vector of joint accelerations $\ddot{q}$ to the joint torque generated by the neuromuscular system. In the other words, the differential equation can be expressed by the equation 2.3.10.

$$D(q, \dot{q}) = N(q, \dot{q}, t) \tag{2.3.10}$$

$D(q, \dot{q})$ represents the passive dynamics of the arm. Similar to robots, passive information such as human skeleton and muscle structure can be written in the following way.

$$D(q, \dot{q}) = M(q)\ddot{q} + C(q, \dot{q}) + g(q) \tag{2.3.11}$$

where $M(q)$ is the inertia matrix of the arm, $C(q, \dot{q})$ is the viscoelastic and friction term, and $g(q)$ is the gravity term. This equation is a well-known equation because

there are many studies about robot dynamics relative to it. Otherwise, $N(q, \dot{q}, t)$ represents the torque generated by neuromuscular activation. This term is assumed to be the function of time and system's state (i.e. q and $\dot{q}$) generally. When human creates a desired action $q_d(t)$, the brain should effectively solve the above dynamics equations and finds $N(q, \dot{q}, t)$. To explore this, researchers first explored how people make the desired action in a state-dependent external force-field $E(q, \dot{q})$. Recent studies demonstrate the hypothesis that people learn forces through the internal model defined in the state space. This internal model may be represented as a field $\hat{E}(q, \dot{q})$, then the dynamics equation is modified by following:

$$D(q, \dot{q}) + E(q, \dot{q}) = N(q, \dot{q}, t) + \hat{E}(q, \dot{q}). \tag{2.3.12}$$

In the fully-leaned phase, the internal model satisfies the following equation.

$$E(q_d, \dot{q}_d) \simeq \hat{E}(q_d, \dot{q}_d) \tag{2.3.13}$$

Furthermore, the researchers explored how people learn time-dependent external force-fields $E(t)$. Surprisingly, there was evidence that people also developed internal models to learn the external dynamics. The internal model is also defined in state space, and the dynamics equation is modified by following:

$$D(q, \dot{q}) + E(t) = N(q, \dot{q}, t) + \hat{E}(q, \dot{q}) \tag{2.3.14}$$

In the fully-leaned phase, the internal model satisfies the following equation.

$$E(t) \simeq \hat{E}(q_d(t), \dot{q}_d(t)) \tag{2.3.15}$$

In this case, the external force may not be completely learned, so people learn and compensate the perturbation by approximating the time-dependent force to internal model.

2.3.2 Combination of motor primitives

As a representative example of the internal model, there is a combination of motor primitive models. One considers the internal model to be a map transforming desired arm trajectories defined in state space into muscle torque or muscle activation through a flexible combination of a set of primitives:

$$\hat{f} = w^T g(x_d, \dot{x}_d, \ddot{x}_d) \tag{2.3.16}$$

where T is the matrix (or vector) transpose operator. $g = (g_1, g_2, \cdots g_m)^T$ is a vector of m scalar-valued primitive functions. g is defined in the state space of the human dynamic system, and state space is expressed to x_d and its derivatives to cover the general human state space (e.g. we can define $x_d(t) = q_d(t)$, where $q_d(t)$ is the joint angle of human arm). $\hat{f}$ is a estimation of exact external force by the combination of primitive functions. Generally, the state where motor primitives are defined $(x_d, \dot{x}_d, \ddot{x}_d)$ is simplified to only the desired velocity $\dot{x}_d$. In this simplification, each primitive function is assumed to have the shape of a Gaussian function inspired from neurons.

$$g_i(\dot{x}_d) = \exp\left(\frac{|\dot{x}_d - c_i|^2}{2\sigma^2}\right) \tag{2.3.17}$$

where c_i's are assumed to be placed in a grid with constant interval. Figure 2.1 shows the diagram of motor primitives and desired trajectory of arm. The internal model is learned through adjusting the weight matrix w, and the learning rule is to minimize $||f - \hat{f}||^2$ where f is the exact external force. The basic update rule is the gradient descent method. Starting from this basic philosophy, there have been many studies on human motor primitives or motor bases.

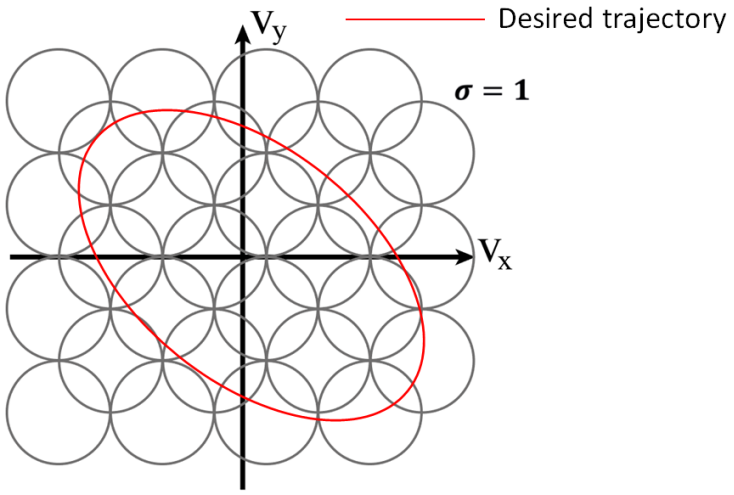

Figure 2.1: Motor primitive arrangement for internal model.

2.3.3 Gain encoding primitives for motor adaptation

The most basic internal model is defined above the state space and is a model that signals motor torque or estimated external force. However, some researchers have begun to argue that the output of the internal model is not an estimated external force, but rather a gain. Joiner et al. assumed a new framework that motor output of internal model is the position gain and velocity gain [11]. When the desired position and velocity profile are x_d and $\dot{x}_d$ respectively, they have considered a model in which input is given by following equation:

$$u = Kx_d + B\dot{x}_d \tag{2.3.18}$$

where K is the position gain and B is the velocity gain. The desired position and velocity profiles refer to profiles in an environment without a force field, and B and K are constant for one task. For the learning of external dynamics, we argue that people learn the gains B and K mentioned above. The learning model uses

a viscoelastic primitive model defined in terms of velocity gain and positive gain two-dimensional space [11]. Each primitive can be expressed by $g_i = (K_i, B_i)^T$, and the resultant gain is obtained by following equation:

$$\begin{pmatrix} K \\ B \end{pmatrix} = \sum_{i=1}^{n} \omega_i g_i \tag{2.3.19}$$

The motor gain value is formed on the primitive side where the activation is large, that is, the weight is large. They concluded that viscoelastic primitive model has correspondence with experimental results, and further the distribution of primitives follows a positively-correlated distribution rather than an unbiased distribution.

The philosophy of learning gain is similar, but a computational model that is different from the previous model has also appeared [8]. They argue that humans motor primitives have anisotropic gain model. Unlike the viscoelastic model above, the primitives are defined on the state space (specially velocity space) similar to the base model, and the output of each primitive is the gain.

$$g_i(\dot{x}_d) = \exp\left(\frac{|\dot{x}_d - c_i|^2}{2\sigma^2}\right) \tag{2.3.20a}$$

$$F_{output} = \sum_{i=1}^{n} \omega_i g_i(\dot{x}_d)\dot{x}_d \tag{2.3.20b}$$

This model focuses on the generalization that occurs when humans learn the force field. For example, in a point-to-point movement, generalization is the theory of how a person manages a force when the force is learned at a slow speed (e.g. 0.3m/s) and then moved to fast speed (e.g. 0.6m/s). Experimental results show that generalization tendency of humans exerts a force of linear extrapolation. Joiner reported that the anisotropic gain model is the best fit to explain this phenomenon [8].

2.3.4 Motor adaptation in circular movement

Most motor learning or human dynamics adaptation studies use the easiest point-to-point task or a simple combination of them. Although humans generate movement of various shapes as well as point-to-point movement in everyday life, it becomes difficult to compare the computational model with the experimental results if the task is slightly complicated in human motor control research. The representative task is circular motion, and research on this has not been done much. In a paper on dynamics adaptation for circular motion, there is a paper about discrete movement and rhythmical movement [25]. Howard found that dynamics adaptation in discrete movement and rhythmical movement uses different mechanisms. In this thesis, the rhythmical circular movement is chosen as the experimental motion, so it has a great deal to do with this part.

2.4 vBOT : robotic manipulandum for studying human motor control

The vBOT system is one of the well-known equipment to explore human motor learning [26]. The system consists of a robotic manipulandum, a monitor, and a mirror. This manipulandum can apply a desired force field to the handle depending on the time, handle's position and handle's velocity. The manipulandum system was turned on while holding the switch attached to the handle, and the subjects were encouraged to keep the switch pressed during each independent experiment. If the subject took a break during the experiment, they would switch it off and hold it again to restart the experiment. The monitor was mounted on the top of the system in a downward direction, and the plane mirror allows the subjects to see

the computer screen. The position of the handle was indicated by a circular cursor of radius 0.5cm through the image of the monitor on the mirror. The height of the mirror can be adjusted according to the eye level of the subject, and the height of the monitor is automatically adjusted so the cursor still indicates the position of the handle. By turning off the lights and proceeding with the experiment, the user can only receive visual information from the screen. The position and the velocity of the handle were recorded in the rate of 200Hz. The whole system is shown in Figure 2.2, where the figure is referenced in [26].

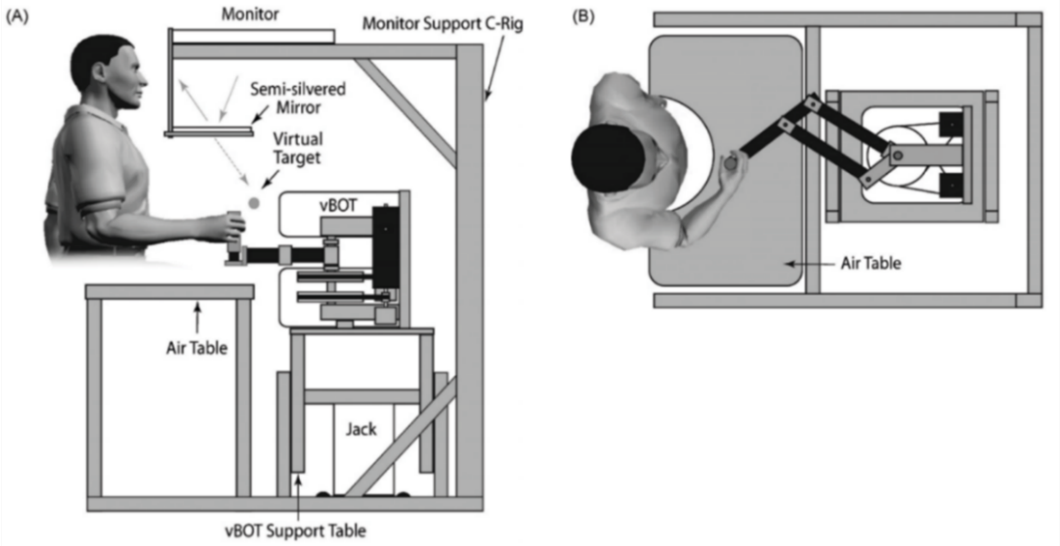

Figure 2.2: The vBOT virtual reality system.

3

Rationale of the Study and Experimental Design

In this chapter, we first present an introductory experiment and its result that leads us to our main hypothesis. Once the main hypothesis is defined, we discuss our experimental idea targetted toward verifying the hypothesis and provide an overview of its implementation. Details of the experimental method will be provided later in Chapter 5.

3.1 Making a movement versus maintaining a static posture

Participants were given a force-field whose direction and magnitude varied with a fixed period (we will call this force-field "time-dependent periodic force-field", see Chapter 4 "External force-field" for details). Experiment 1 was designed to explore how participants learn the time-dependent periodic force-field. Two tasks were performed in series, whose order was counter-balanced across the participants: 1) the

"hold" task: participants were asked to hold the the cursor (i.e. the robotic handle) statically to the centre of a time-dependent periodic force-field, counteracting the perturbing radical forces and 2) the "draw" task: participant were asked to draw a small circle (radius = 1.2 cm) with a same frequency to an imposed time-dependent periodic force-field. A schematic diagram of the tasks is shown in Figure 3.1.

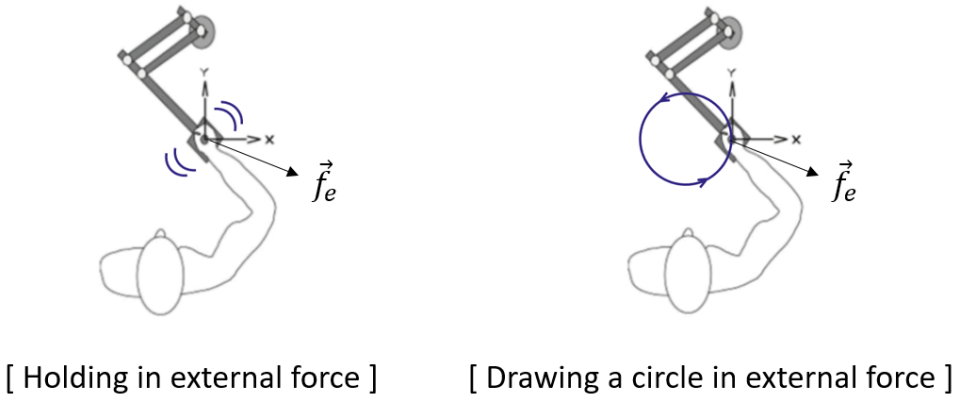

Figure 3.1: Diagram of the "hold" task and "draw" task for Experiment 1.

If participants are able to develop a predictive control strategy to cope with the given periodic force field, beyond a purely reactive strategy mainly based on the co-contraction of muscles, the "hold" task can be considered as a classical adaptive control problem, where a controller is required to learn the periodic external forces and to develop a counteracting control strategy generating time-dependent (i.e. periodic) control forces in the opposite direction to the external force. For the "draw" task, there are two possible choices of control strategy: First, the same counteracting periodic control strategy can be incorporated. Alternatively, since the frequency of circle-drawing is synchronized to that of the external force, the

periodic force-field can be regarded as an angle-dependent force field. A possible control strategy in such case would be a state- (i.e. angle-) dependent controller with no time-dependency.

Based on these assumptions, comparison of the performance in two tasks will inform us as to what kind of control strategy the participants were able to develop during the experiment. If participants developed a periodic time-dependent control strategy, it is clear that the performance of the "hold" task will be equal or higher than that of the "draw" task, since the developed control strategy during the "draw" task may interfere with ongoing movement that adds extra motor noise to the system. If participants developed a state-dependent control strategy, we expected that the participant will outperform in the "draw" task, while the performance of the "hold" task will be no higher than that of purely reactive control strategy. This is because the "hold" task by definition requires the controller to maintain a single state, i.e. a single position with zero velocity, and therefore makes it impossible to establish any equivalent state-dependent control strategy. Figure 3.2 will help you understand these assumptions and expected results. Repeated action to learn is represented as a fixed desired trajectory in the state space. The figure shows only the velocity space in the state space. For the state-dependent force field, the external force is given at each point of the desired trajectory. In the view of state-space learning, participants would compensate the external force while estimating the given force for each point of the desired trajectory.

Figure 3.3 shows the radial error at fully-learned phase of each sub-experiment

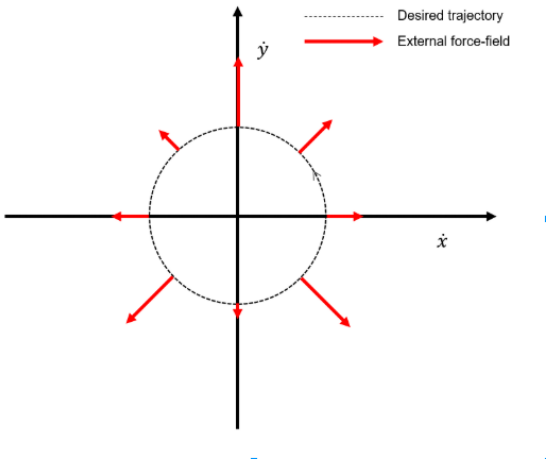

Figure 3.2: Task's desired trajectory in the state space and external force-field.

of subject 3. We average trajectory data piece-wisely for each sub-experiment's result from Experiment 1. We averaged each result over the last 30 trials. Figure 3.3-A shows the error profile when participants perform "draw" task during no force-field. Figure 3.3-B shows the error profile when participants perform "hold" task during the time-dependent force-field. Figure 3.3-C shows the error profile when participants perform "draw" task during the time-dependent force-field. We could see that the "hold" task seems not to learn external force-field from the radial error (Figure 3.3, B). However, while there is little difference in radial error profile between with and without force-field (Figure 3.3, A and C), the "draw" task can be seen as learning force-field. A direct comparisons of the error profiles of "hold" task and "draw" task can be concluded that the latter has learned much more about the force field. The same tendency was observed for other subjects. As a result, we can confirm that the hypothesis proposed above is demonstrated.

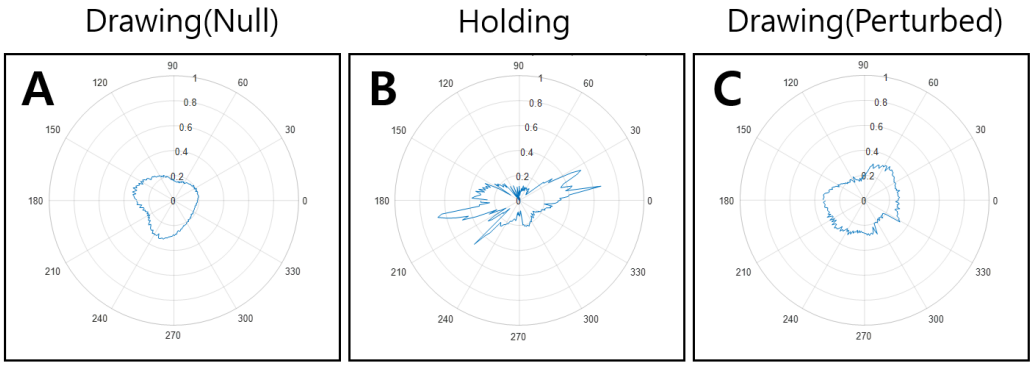

Figure 3.3: Radial errors at late exposure phase (cycle 70 - 100) when stabilizing from perturbation.

3.2 Experimental design and thesis statement

The participants were seated and grasped the handle of a planar robotic manipulandum with their dominant hand. Handedness was balanced across the participants, i.e. 5 subjects were right handed and the rest were left handed according to the Edinburgh handedness inventory. All participants had no reported neurological disorders. After a brief familiarization period, participants were asked to make circular movements along a reference circle displayed on the screen in a constant frequency, indicated by a tone or by a target cursor movement depending on the type of the experiment. While making circular movements, external forces were applied to the handle in the radial direction, disturbing participants from drawing smooth circles, and participants were instructed to cope with the perturbing forces to minimize the deviation of the cursor from the reference circle, while maintaining the required frequency. In this setup, three experiments, described below, were conducted which were specifically designed to test the following two hypotheses: (1) The internal model is learned as state-dependent feedback response and but

does not have a time representation. (2) More complex internal models require larger capacities in state-space for encoding, i.e. faster movements.

4

Results and Discussion

In this chapter, we provide the result of our study. We first propose several measures of adaptation, either taken from the literature or developed by ourselves, that estimate the performance of motor learning. After that, we provide detailed analyses comparing the performances of learning in different encoding capacities or varying complexities, and discuss whether the proposed hypothesis can be validated by our experimental result. Finally, we discuss the broader implication of the result in general human motor control and potential issues.

4.1 Trade-off between encoding capacity and signal dependent noise

4.1.1 Expansion of logic: encoding capacity

From Experiment 1's result, it was shown that developing the reference trajectory would help in learning the force-field by forming a capacity in the state-space.

After observing this results, a natural question arises that how the capacity of the desired motion in the state space relates to the degree of learning external force-field. In this paper, we defined the terms "encoding capacity" and "encoding error" for clarity. The encoding capacity meant some measure of the desired trajectory D(e.g. the length or the closed loop volume) in the motion's state-space. The name "capacity" came from the philosophy of storing information of force fields. When force-field was encoded in the encoding space, there must be some error between stored force-field information and exact perturbing force-field. We defined this error as the encoding error. If the estimated force from stored information is $\hat{f}(\dot{x})$ and external force is $\vec{f_e}(\dot{x})$, encoding error(EE) was expressed as the equation 4.1.1.

$$\text{EE} = \int_D ||\hat{f}(\dot{x}) - \vec{f_e}(\dot{x})||^2 dl \tag{4.1.1}$$

The motivation for Experiment 2 was to examine the relationship between encoding capacity of the required task and the encoding error for the given force-field. There are total six sub-experiments according to the movement speed, and all sub-experiments were designed so that the encoding capacity in the position space were constant and encoding capacity in the velocity space were different (see Chapter 4 "Experiment 2" for details). We test the hypothesis that as the encoding capacity increases, encoding error decreased and degree of learning increases.

We used a force-field that depends on the current hand state of the participant, unlike the time-dependent force-field of Experiment 1 (we will call this force-field "state-dependent force-field", see Chapter 4 "External Force Field" for details). The first reason for using different force fields is that time-dependent periodic force-field is exactly equivalent to the state-dependent one when the participant's hands perform a constant velocity motion with the same periodic force-field. In

Experiment 1, the goal was to compare the degree of learning between holding task with the drawing circle task, so it was inevitable to use time-dependent force-field. However, in the Experiment 2, we wanted to show the correlation between encoding capacity and encoding error, so we removed the time-dependency that is not related to learning and reconstructed the experiment so that force profiles were state-dependent.

In terms of the multiplicative noise, drawing error would be expected to increases as the hand velocity increases. In conclusion, we can expect that the minimum error can be achieved at a certain middle hand velocity. The graph of drawing error over rotation period will have the tendency of convex function so that there will be optimal rotation period.

4.1.2 Experimental results for radial force

Figure 4.1 shows the hand trajectory of each sub-experiment at fully-learned phase of subject 4. As we expected, the experiment result of the actual error had the tendency that the hand speed which minimizes the error exists in the middle, not both ends. In other words, the hand trajectory at both ends of the period had a large error. In addition, we observed that the aspects of the error were different at both ends. When the speed was slow, the variance of the trajectory was large (Figure 4.1, A). However, when the hand speed was fast, the variance was small but the shape itself was rugged (Figure 4.1, E).

Figure 4.2, 4.3, and 4.4 show statistical graphs of the results of Experiment 2. The learning curve was drawn for 0.7 second, 1.0 second, 1.3 second, and 2.0 second as new experiments were conducted (experiment configuration is not differ from before). The graphs show the learning curve for each rotation period when the complexity index is 1, 2, and 3, respectively. The error metric was determined

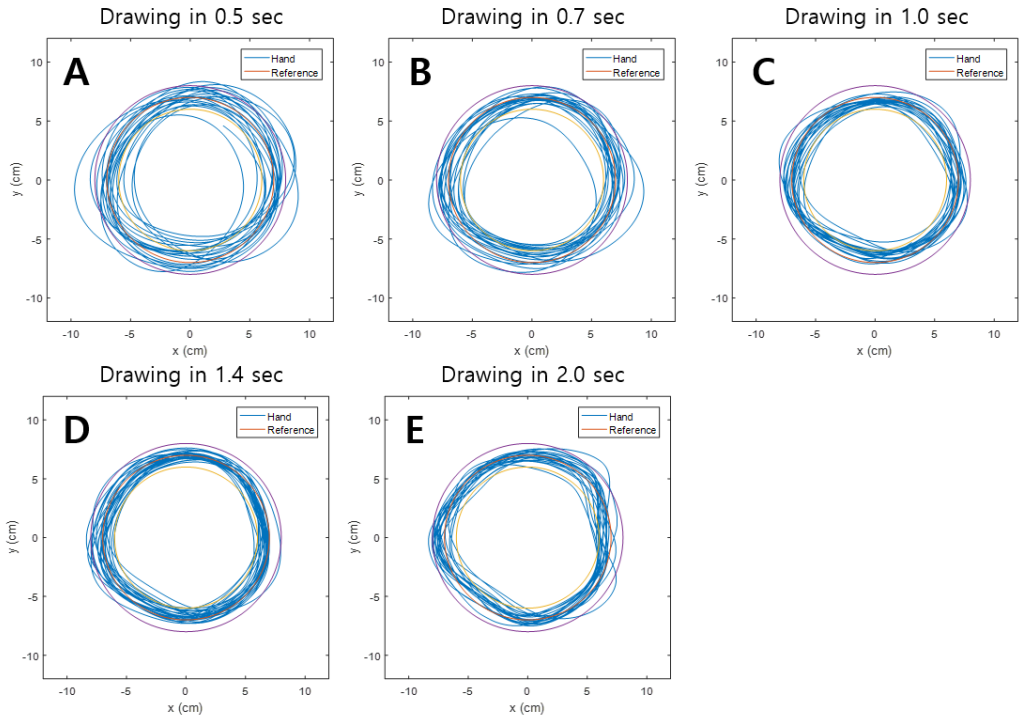

Figure 4.1: Hand trajectory of each sub-experiment of Experiment 2.

by integrating over time the value obtained by subtracting the actual trajectory of the hand from the desired trajectory radius for each cycle. As can be seen from the Figure 4.2, it can be seen that the error level is saturating at a point that does not differ significantly from period to period. However in the Figure 4.3 and Figure 4.4, the higher the complexity index and the faster the cycle, the smaller the error level clearly. These results fit our hypothesis exactly, and we will explain about the reason. As saying above, we have hypothesized that the faster the speed, the stronger the signal-dependent noise effect, but the higher the degree of learning. When the complexity index is 1, the force field is relatively easy to learn, so it can be thought that motor learning has occurred to some extent in all periods. So the

error level did not differ greatly in Figure 4.2. This tendency is that the effect of signal-dependent noise is mixed with the learning effect. However, as complexity index becomes 2 or 3, saturation occurs at the lowest error level at period 0.7, which is the fastest. If there is only a signal-dependent noise effect and no learning effect, the result should be reversed. However, as a result, we can argue that there is a lot of force-field learning at a fast pace. We can see that overall saturation occurs rapidly in the exposure phase, independent of comparing with each period, and there are not many after effects. To confirm this, we have also experimented with tangential forces rather than radial forces, and we will discuss them in the next section.

Meanwhile, we put some catch trials in the middle of the experiment. It is difficult to tell from the fact that the position error has a lot of complex influences, so learning is actually done. Particularly in this thesis, more complex factors are mixed because the cycle is to compare the learning degree for different experiments. In conventional motor adaptation papers, a catch trial is mixed in the middle of the experiment to confirm the degree of pure learning. The catch trial used a null field previously, but recently it has directly measured the force learned using a spring-damper system. Existing experiments are easy to implement a catch trial because it is a discrete movement experiment of a straight line. However, it is very challenging try to implement a catch trial in continuous circular motion, and there is no paper related to it. We designed and implemented a new catch trial that can be applied to continuous circular motion (see Chapter 4 “Catch trials for circular movement” for details). The plot of the human force estimate for the case of complexity index 3 through the catch trial is shown in the Figure 4.5. The catch trial results for the other complexity indices are in Figure 4.6 and 4.7. The blue line is the force-field to learn, and the red line is the force-field learned.

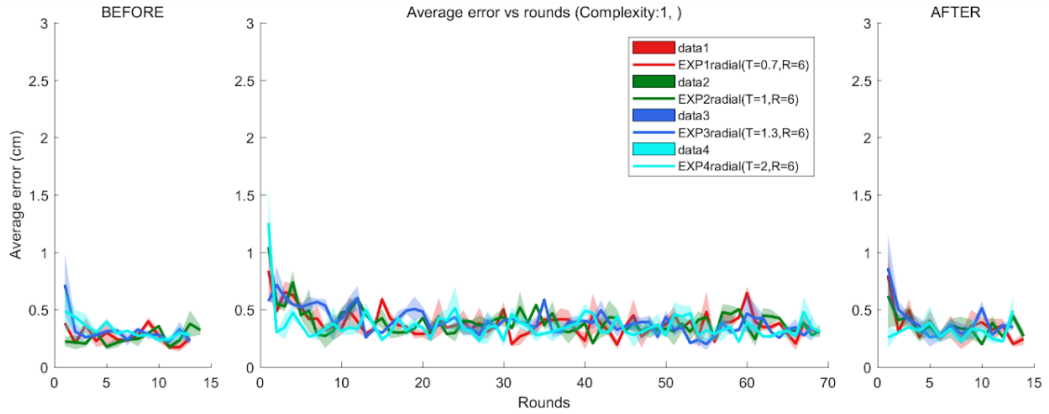

Figure 4.2: Learning curve of Experiment 2 at complexity index 1.

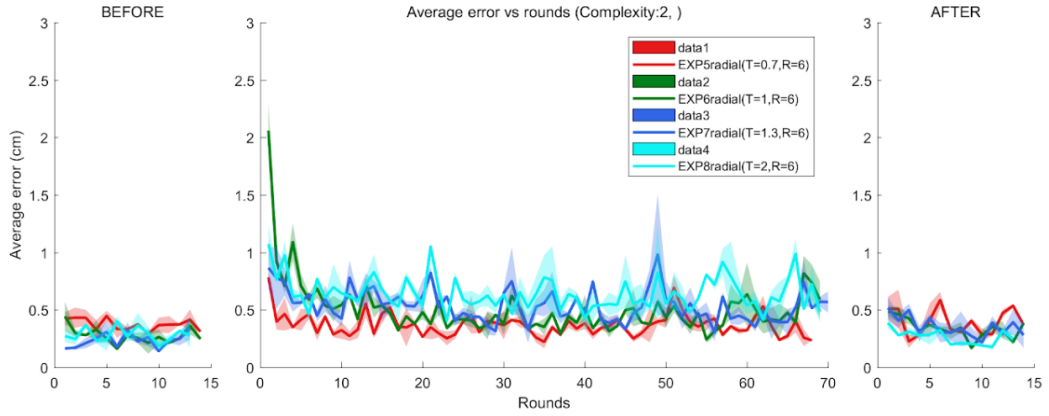

Figure 4.3: Learning curve of Experiment 2 at complexity index 2.

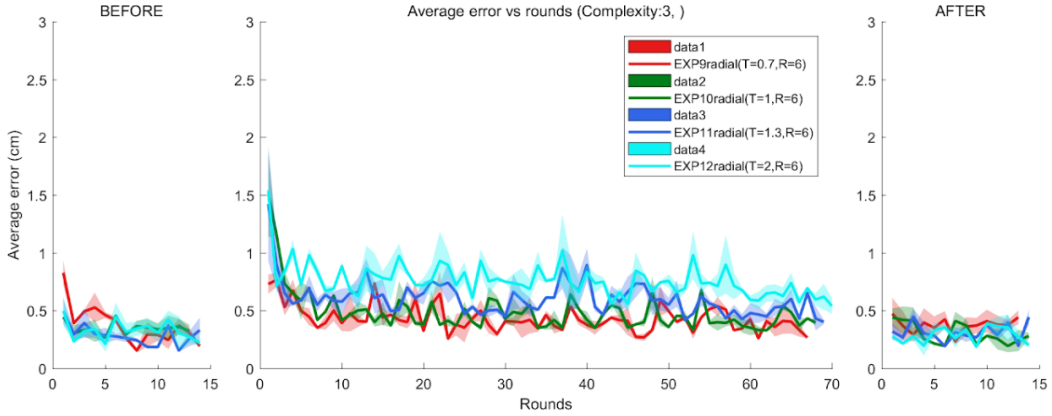

Figure 4.4: Learning curve of Experiment 2 at complexity index 3.

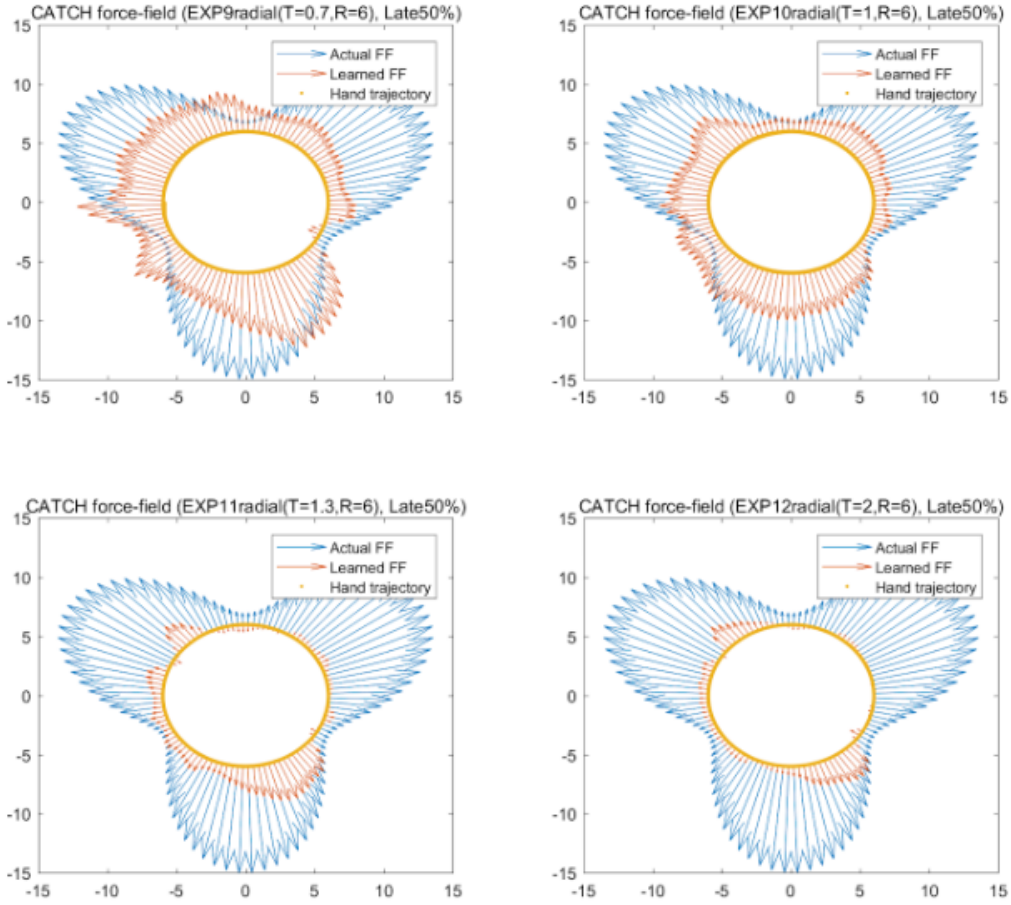

Figure 4.5: Estimated radial force of Experiment 2 at complexity index 3.

As you can see, we can see that more force-field learning occurs at faster speeds. Although subjects did not learn the force-field completely, their leaned force-field reflect the curvature of the original force-field. It was confirmed that no force was shown in the catch trial in the pre-exposure state, in which nothing was learned. Figure 4.8 is the result of plotting the compensation error when the force-field is fully learned according to the complexity index. It can be more intuitively seen

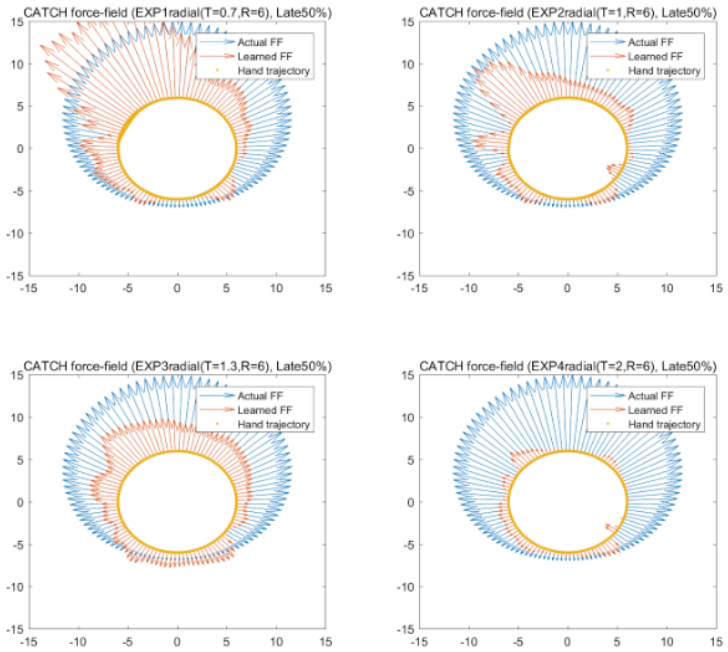

Figure 4.6: Estimated radial force of Experiment 2 at complexity index 1.

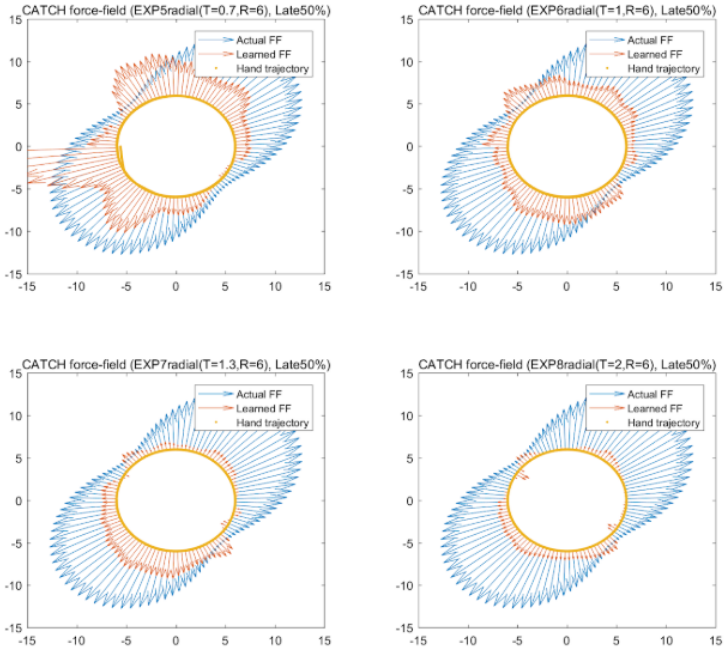

Figure 4.7: Estimated radial force of Experiment 2 at complexity index 2.

that the tendency to learn the force better at faster speeds in all complexity indices. So we have a high confidence that the above figures mean purely learned force-field. The fact that they learn better as they get faster is confirmed not only by position errors, but also by catch trials.

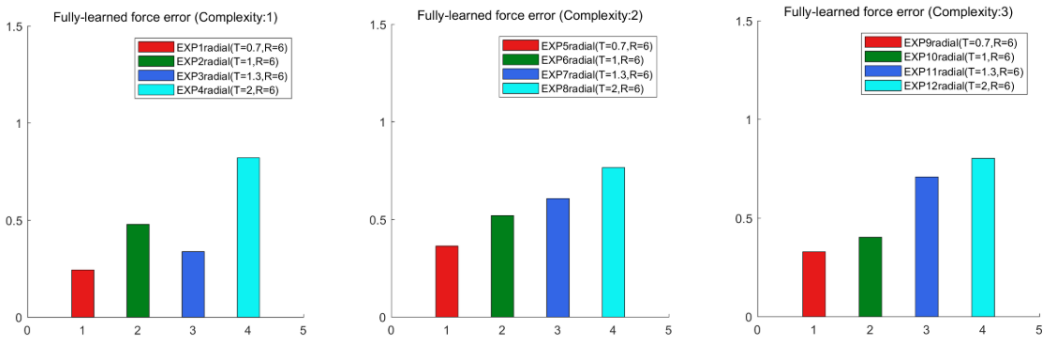

Figure 4.8: Force compensation error at each complexity index.

4.1.3 Experimental results for tangential force

As mentioned briefly in the previous section, learning was quick for radial force compensation and the learned force was quickly washed-out. So we tried the same experiment on the tangential force. Tangential force refers to a force parallel to the direction of travel when a perfect circle is drawn. The results of the experiment on each complexity index for the tangential force are shown in Figure 4.9, 4.10, and 4.11. As can be seen, the shape of the learning curve in the exposure phase is more prominent than that of the radial force. Furthermore, the shape of the learning curve in the exposure phase is more prominent than that of the radial force. Even in this case, the discussion in the previous section can be applied equally. The larger the complexity index is, the smaller the tendency is when the error level is faster when saturation is achieved. In addition, The fact that the faster the speed,

the more the after-effect occurred, supports the fact that more force-field learning occurred. Since the tangential force is a force parallel to the direction of travel, the above catch trial can not be applied. So the catch trial results are omitted.

4.1.4 Discussion : radial force versus tangential force

As can be seen from the above results, the learning curve shows different patterns for both radial and tangential forces. More specifically, it can be concluded that the learning of the tangential force tends to appear more slowly. In our results, there are advantages and disadvantages when using each force. Using radial force, learning takes place quickly and does not get a typical learning curve, but the newly learned catch trial can be used to directly measure the force learned by the subjects. Conversely, when using tangential force, the learning curve appears more clearly, but it is difficult to observe direct learning because the catch trial is not available. No papers have been published on the adaptation of radial and tangential forces in circular motions. In this thesis, the study was conducted in extreme cases where there is only tangential force and only radial force. In general, the force field used in motor adaptation studies is either a curl-field or a skew-curl field, and both radial and tangential forces are present when circular motion is applied. Therefore, studying whether to learn independently or interacting with each other when there are two forces is also considered to be impact future work.

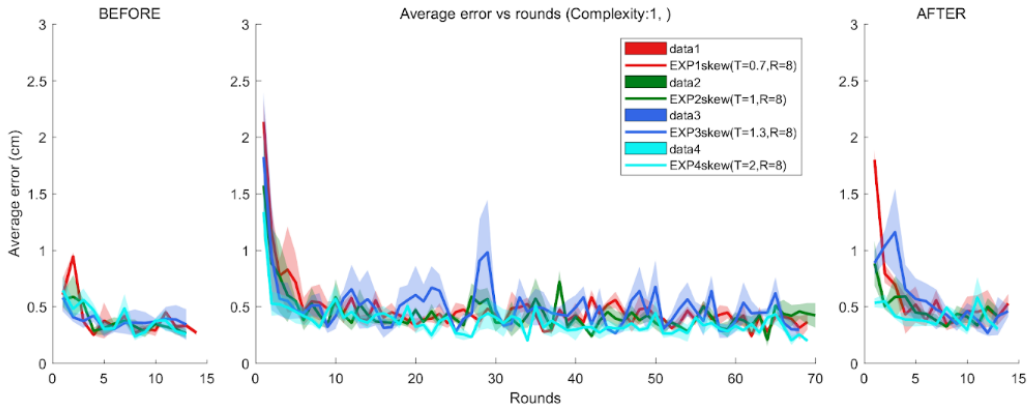

Figure 4.9: Learning curve of tangential force-field at complexity index 1.

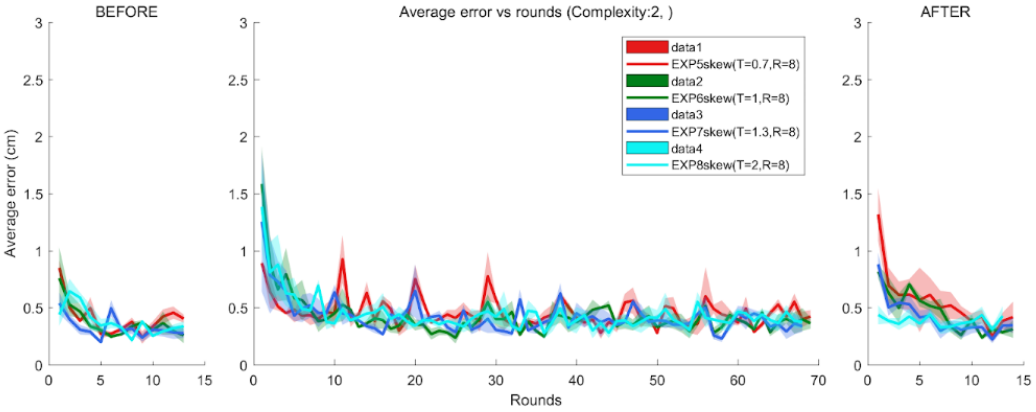

Figure 4.10: Learning curve of tangential force-field at complexity index 2.

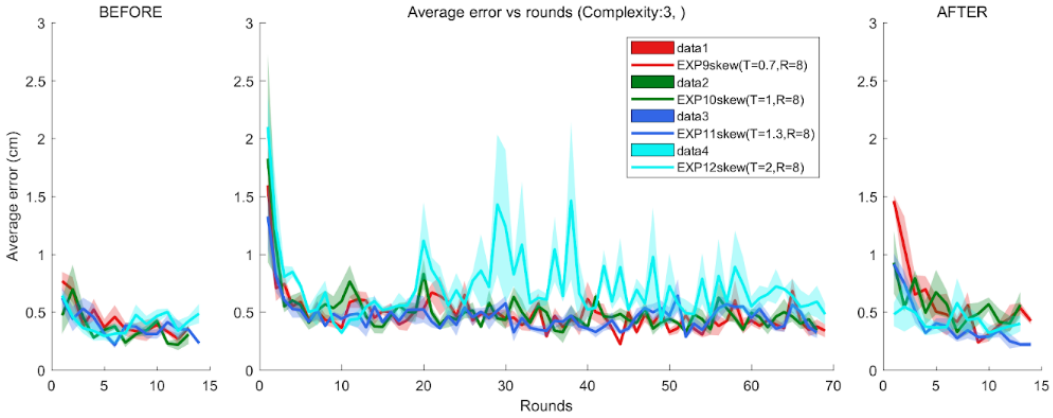

Figure 4.11: Learning curve of tangential force-field at complexity index 3.

4.2 Influence of the mechanical factors during adaptation

4.2.1 Mechanical rebuttal for result analysis

We found that the average error in the "draw" task was smaller than the error in the "hold" task. In the other words, making a reference trajectory and following it was more stable than holding a static point. The results were consistent with the claim that human could learn the force field in the state space. However, there could be a mechanical rebuttal to these results. It was claimed that the participants hand would have momentum by tracking a reference trajectory (i.e. the momentum is the product of mass and velocity in the point mass case), thus they could keep the stability from the external force. In order to test the influence of this rebuttal, we designed a new experiment Experiment 3 (see Chapter 4 "Experiment 3" for details).

4.2.2 Experimental results and discussion

We additionally experimented by fixing the period of the time-dependent force-field and slightly faster hand speed. In this case, hand speed and force-field's period do not match. We compared the results of this asynchronized experiment with the results of the synchronized experiments. Figure 4.12 shows the hand trajectory two sub-experiments, synchronized and asynchronized case at fully-learned phase. From the figure, we observed that the accuracy get worsened if we move hand faster in the identical force-field. In the other words, second sub-experiment's average error is bigger than first sub-experiment's average error in Experiment 3, and we could say that the subjects can not learn the force-field in asynchronized case. If the influence of the above rebuttal was large enough, the circle should be drawn well in asynchronized case because of the increased hand velocity. We can

conclude that this criticism is not valid in Experiment 2's result, and the concept of state space learning has a dominant influence on these whole experiments. Figure 4.13, 4.14, and 4.15 show statistical graphs of the results of Experiment 3.

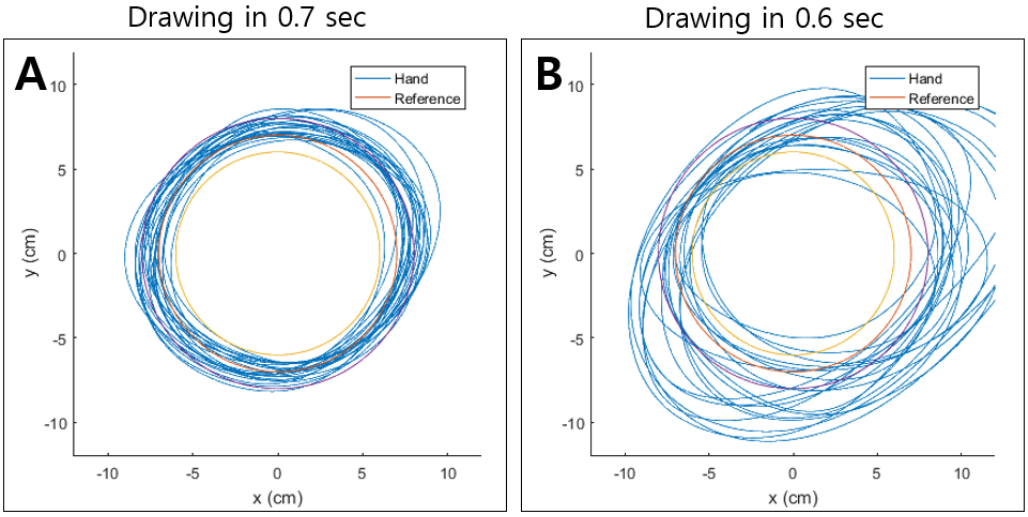

Figure 4.12: Hand trajectory of each sub-experiment of Experiment 3.

The learning curve was drawn for 1.0 second, as new experiments were conducted (experiment configuration is not differ from before). The graphs show the learning curve for rotation period 1.0 second when the complexity index is 1, 2, and 3, respectively. In all figures, the red graph is the graph when the force-field and rotation period are synchronized, and the green graph is asynchronized. Overall, it has been confirmed that the error level is larger when it is asynchronized in all cases. The more we can see, the smaller the complexity index (i.e. the simpler the force-field), the greater the difference between the two error levels. According to our assumptions, when the periods are asynchronized, we do not learn the force-field at all. If the error levels of the two error graphs are large, it implies that

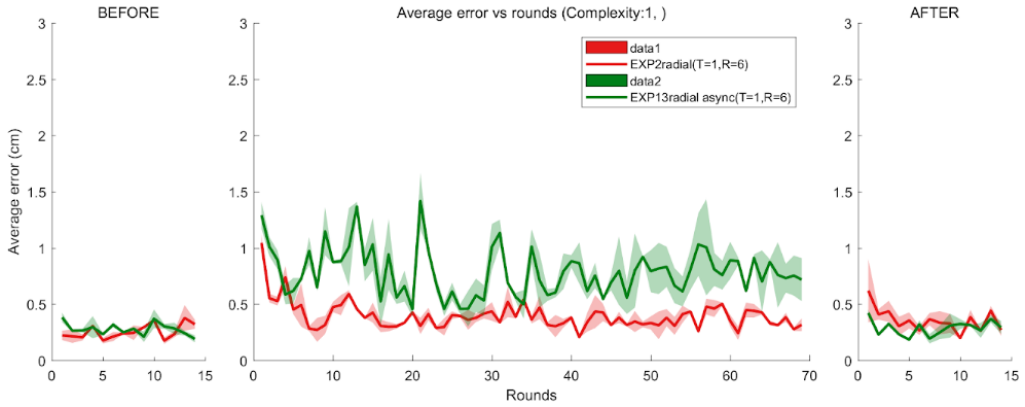

Figure 4.13: Learning curve of Experiment 3 at complexity index 1.

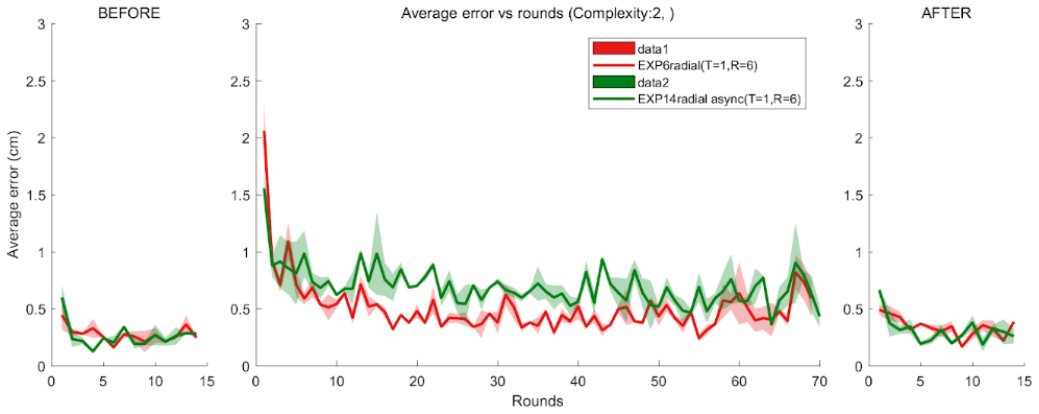

Figure 4.14: Learning curve of Experiment 3 at complexity index 2.

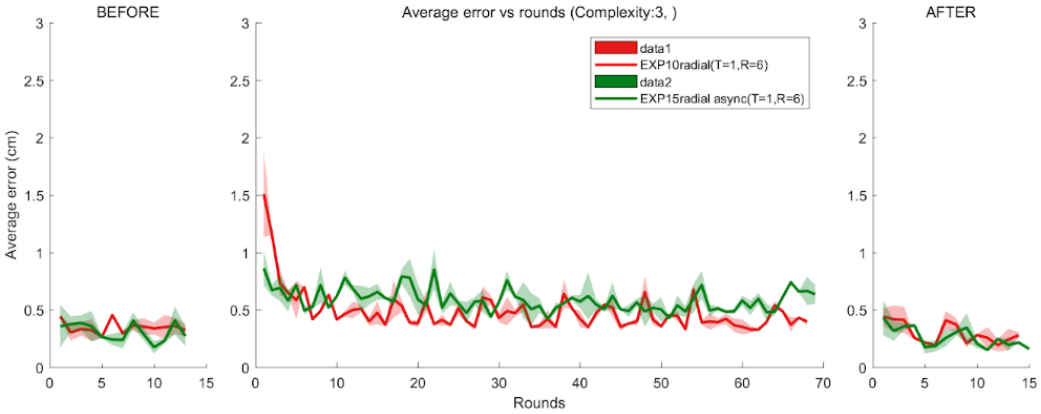

Figure 4.15: Learning curve of Experiment 3 at complexity index 3.

learning will be more when synchronized. From these results, we can completely counter the rebuttal that the mechanical effect may dominate the experimental results. There is one more fact that can be proved through these experimental results. The point that always becomes an issue when looking at the position error is the person's co-contraction or stiffness. In this case, one might argue that the degree to which a person stiffs a handle will have a significant impact on error. However, if co-contraction is dominant, the error level of the synchronized case and the asynchronized case should be similar. Since the result is not so, we have also found that the experiments conducted by this thesis are not significantly affected by co-contraction.

4.3 Simulation results using motor primitives

4.3.1 Problem definition

We verified experimental results with simulation model. To simulate the internal model, we used the motor primitive framework which is a representative model of the internal model parametrization. We solved an optimization problem 4.3.2 to observe the encoding error when external force-field was fully learned.

$$\min_{w} \int_{D} ||\hat{f}(\dot{x}) - \vec{f_e}(\dot{x})||^2 dl \tag{4.3.2a}$$

$$g_i(\dot{x}) = \exp\left(\frac{|\dot{x} - c_i|^2}{2\sigma^2}\right) \tag{4.3.2b}$$

$$g = (g_1, g_2, \cdots g_m) \tag{4.3.2c}$$

$$\hat{f}(\dot{x}) = w^T g \tag{4.3.2d}$$

D is the desired trajectory in velocity space, and c_i's are assumed to be placed in a grid with constant interval like previous researches [5, 6].

4.3.2 Simulation results

The simulation results are shown in Figure 4.16 and Figure 4.17. Figure 4.16 shows the encoding error at fully-learned phase according to the movement period. Since the signal dependent noise effect is not reflected, it is correct that the tendency to increase monotone increases. Simulation results are shown more in-

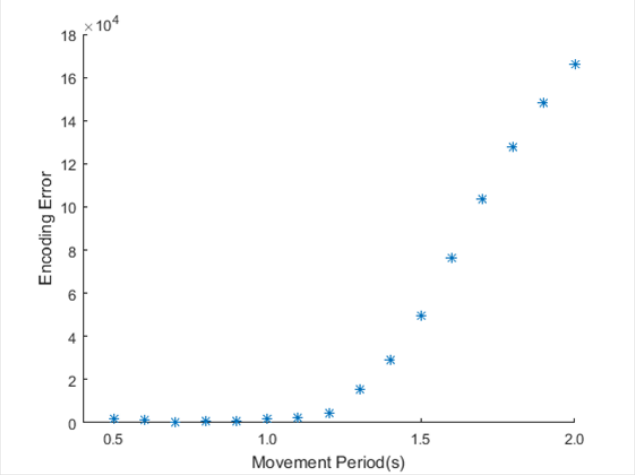

Figure 4.16: Encoding error-period graph at simulation.

tuitively in Figure 4.17. Figure 4.17 shows the real force-field which is blue vector field and estimated force-field which is orange vector field, and the activation which means the value of weight corresponding to each primitive function. From the figure, we can see the tendency that motor primitives estimate real force-field well as motion speed increases (Figure 4.17, A and B). Additionally, as rotation period decreases, motion speed increases and motor primitive functions' space covers bigger space. Covering a larger space increases the expression power of the learned external force because it can activate as many motor primitives as human can. This fact is also shown in the figure (Figure 4.17, C and D). These inferences

support the fact that the encoding error decreases as the hand velocity increases.

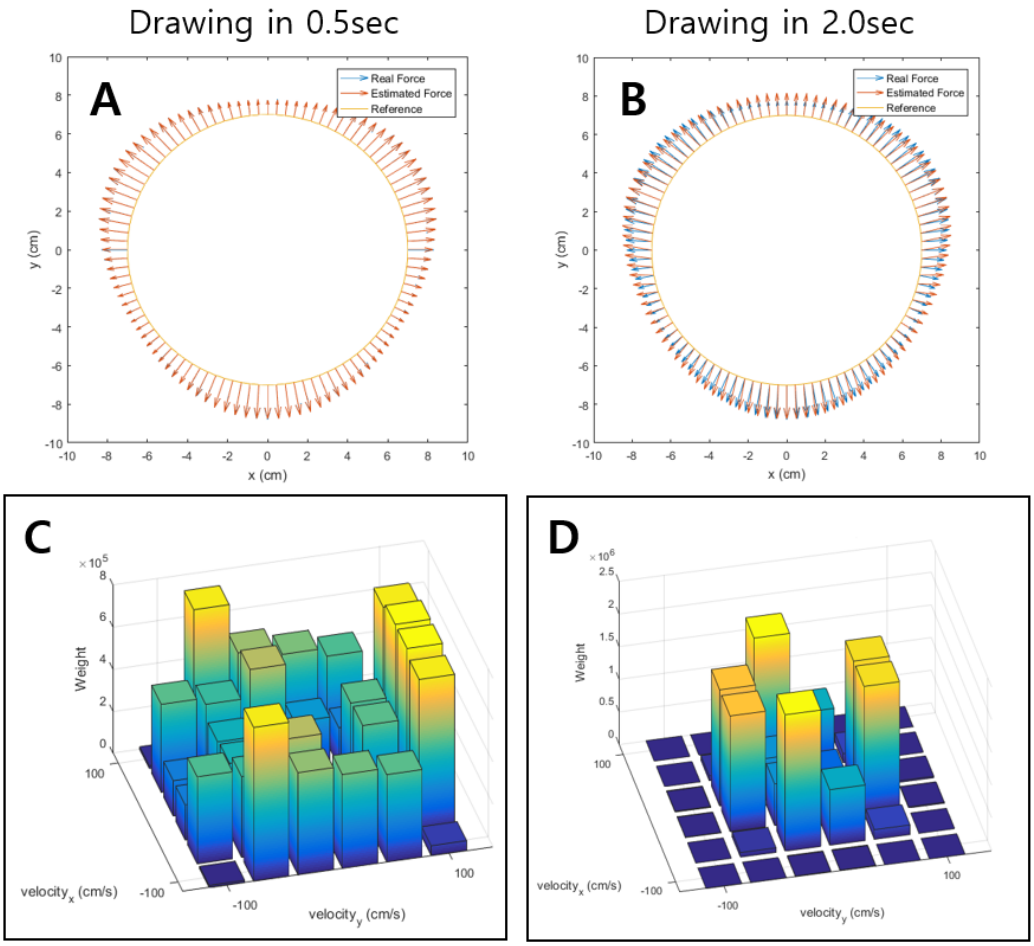

Figure 4.17: The motor primitive simulation results of Experiment 2.

5

Experimental Methods

In this chapter, we present the detail of methodologies used in the experiments. Experimental method has already been explained briefly, but here we present specific experimental methods so that other researchers can reproduce the experiment. We introduce the external force-field used in the experiment and the specific procedure of each main experiment. Particularly, a new catch trial model, which is well applied in continuous circular motion, is proposed.

5.1 General task

The participants were seated in a dark room and grasped the handle of a planar robotic manipulandum(vBOT) with their right hand. The vision of the hand and the manipulandum was blocked, but a veridical visual feedback of the handle position was provided as a circular cursor by a horizontally mounted monitor viewed through a mirror.

5.2 External force-field

Throughout the experiment, two types of the force-fields were applied to the handle while making circular movements. In the Experiment 1 and experiment 3, a time-dependent periodic force-field is applied to perturb the hand. The applied force is expressed by the following equation:

$$\vec{f_e} = (a + b \sin n\omega t) \begin{pmatrix} \cos \omega t \\ \sin \omega t \end{pmatrix}. \tag{5.2.1}$$

The parameters a and b meant the mean and amplitude of the periodic force-field. We fixed the parameters as $a = 5$ and $b = 2$ which . The parameter ω meant the angular velocity which determines the period of the force-field with the equation $T = 2\pi/\omega$. The parameter n was introduced in order to adjust the difficulty of the degree of learning of the force-field. Since the complexity of the force-field is determined by the parameter n, we will refer to n as the complexity index. In the Experiment 2, a state-dependent force-field is applied as the following equation:

$$\vec{f_e} = (a + b \sin n\theta) \begin{pmatrix} \cos \theta \\ \sin \theta \end{pmatrix} \tag{5.2.2}$$

$$\theta = \text{atan2}(y, x). \tag{5.2.3}$$

The force-field's mean, amplitude, and complexity index were similarly defined with the time-dependent periodic force-field. The parameters a and b were fixed for the same value with Experiment 1 and 3. The state values x and y were the current position of the handle, and the polar coordinate angle θ is the angle in the Euclidean plane, given in radian, between the positive x-axis and the ray to the point $(x, y) \neq (0, 0)$. If the subjects drew circles at the constant angular velocity ω relative to the origin $(0, 0)$ in this force-field, they could feel the same

effect of receiving a time-dependent periodic force-field with ω. The profile of the force-field according to the complexity index can be seen in Figure 5.1. In the case of tangential force, a force-field is used which is rotated counterclockwise by $\pi/2$ in the above force field. The equation of the force-field is as following:

$$\vec{f_e} = (a + b \sin n\theta) \begin{pmatrix} -\sin\theta \\ \cos\theta \end{pmatrix} \tag{5.2.4}$$

$$\theta = \text{atan2}(y, x). \tag{5.2.5}$$

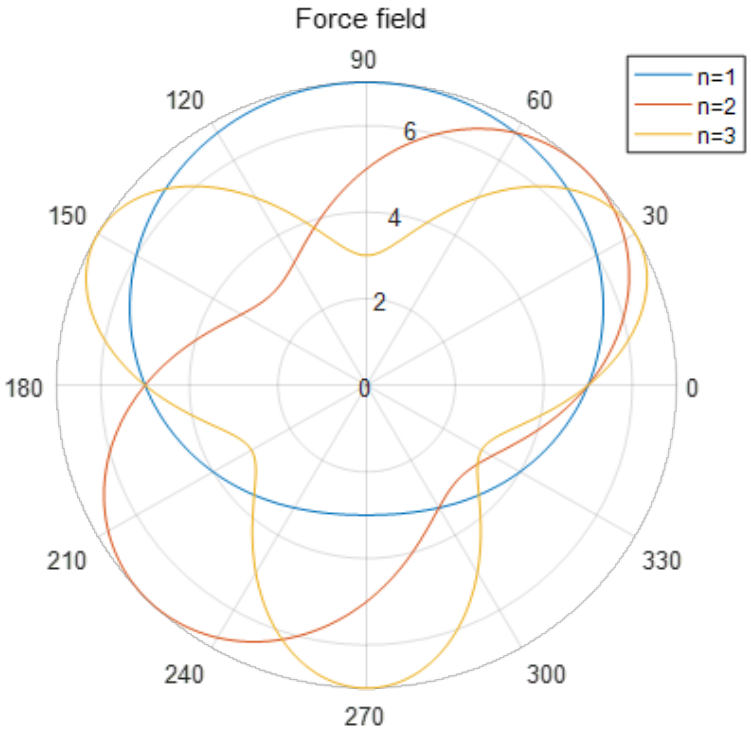

Figure 5.1: Force-fields according to complexity index.

5.3 Main experiments

5.3.1 Experiment 1

Experiment 1 consisted of three sub-experiments. In the first sub-experiment, participants were asked to follow a target cursor that rotated a reference circle with a radius of 1.2 cm and with a frequency of 0.6 seconds per cycle. Subjects perform task following the target for 33 laps during no force-field. This sub-experiment's result would became baseline for data analysis. In the other two sub-experiments, External time-dependent force-field was applied to hand grasping manipulandum. Complexity index was chosen to be 2, and force-field's period was 0.6 seconds or $\omega = 2\pi/0.6$. In the second sub-experiment, subjects performed the task of holding their right hands at the origin point while grasping the manipulandum and resisting the force-field. There was a circle with a diameter of 0.5cm centered on the origin point. When the distance between the origin point and the manipulandum cursor was less than 1cm, it was green. When it was more than 1cm, it was red. Subject were instructed to keep the cursor's color to be green. They performed this task for 90 seconds, and the score increased when the color was green and decreased when the color was red. In the third sub-experiment, subjects performed the task of following the rotating target with period 0.6 seconds, which is the same value of force-field's period, and radius of rotation 1.2cm, and the diameter of 0.5cm. There was also a circle with a diameter of 0.5cm centered on the origin point. The same force-field was applied in the sub-experiment. When distance between the rotating target circle and the manipulandum cursor was less than 1cm, circle of origin was green. When the distance was more than 1cm, it was red. Subject were instructed to keep the cursor's color to be green. They performed this task for 90 seconds or 150 rotation laps, and the score increased when the color

was green and decreased when the color was red. Between each sub-experiment, subjects take a short break for 3 minutes.

5.3.2 Experiment 2

Unlike Experiment 1, there was no rotating target circle. Instead, reference circle band with center circle's radius 7cm and band's width 2cm exist. In this experiment, external state-dependent force-field with complexity index 3 was applied to hand grasping manipulandum. Subjects performed the movement of drawing circle with their right hands while grasping the manipulandum. When the manipulandum cursor was positioned inside the reference circle band, the reference circle band's color became green. When it got out of the band, it was red. The experimental display in Experiment 1 and Experiment 2 is shown in Figure 5.2. Subjects were instructed to draw reference circle keeping the band's color to be green at each period: 0.5, 0.7, 1.0, 1.4, 2.0, and 2.8 seconds. At each desired period, a periodic bip-bop sound of the same period is given so that subjects can be assisted in drawing the circle. If the desired period is less than 1 second, the bip-bop sound is given 1 time in each rotation cycle, 2 times if more than 1 second and less than 2 seconds, and 4 times if it is more than 2 seconds. In each period, The experiment consists of three phases : pre-experiment, main-experiment, and post-experiment. In pre-experiment, subjects drew reference circle for 30 laps in no force-field. In main-experiment, subjects instructed to draw reference circle for total 150 laps at each desired period in given state-dependent force-field above. The entire composition of the experiment is summarized in Figure 5.3. The experiment includes a combo score to motivate the force-field learning, so if you succeed in rotating one circle at desired period, your score will increase by 1, and if it fails, it will not increase. The catch trials appear pseudorandomly every 10 times during

the main-experiment. The meaning of the catch trial and its reason for existence are explained in the "Catch trial" section. After the main-experiment is over, it goes to the post-experiment phase. Subjects drew reference circle for 30 laps in no force-field again similar to pre-experiment. In order to avoid the order effect, we randomly suffle the order of 6 sub-experiments according to the period. Between each sub-experiment, subjects take a short break for 3 minutes.

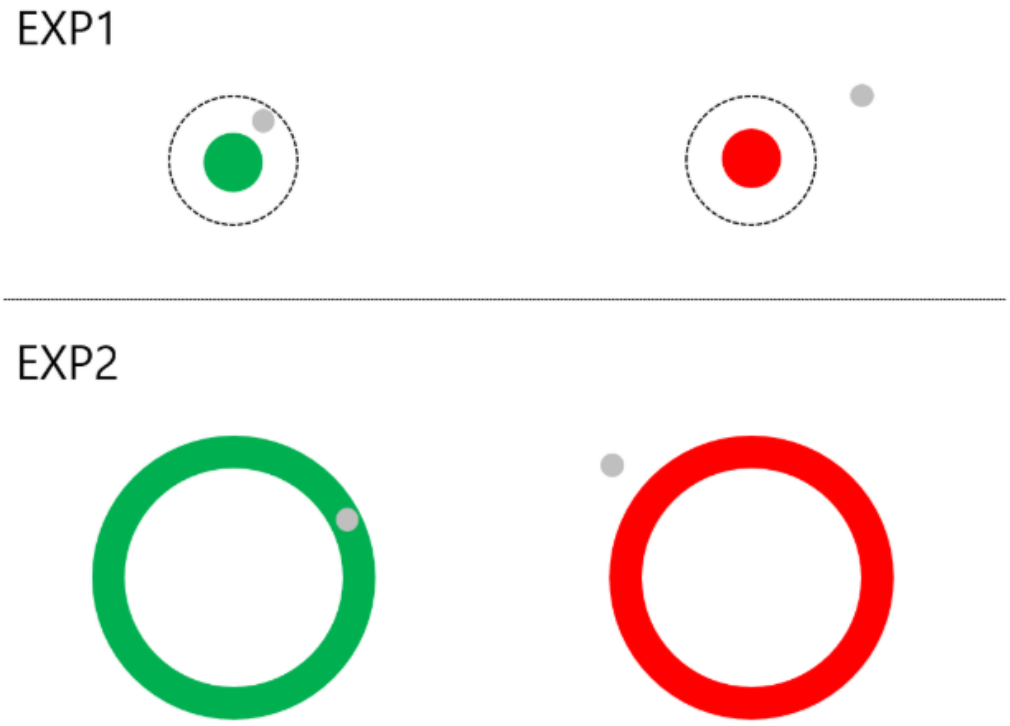

Figure 5.2: Diagram of home position (Experiment 1) and reference circle band (Experiment 2).

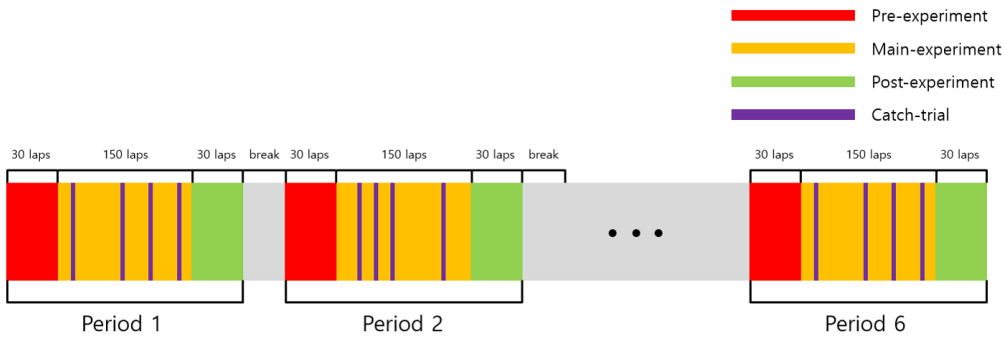

Figure 5.3: Experimental composition diagram of Experiment 2.

5.3.3 Experiment 3

Subjects were instructed to draw the reference circle with a radius of 7cm with band's width 2cm. The setting is almost similar to Experiment 2, but the force-field type was the time-dependent force-field with complexity index 2 in Experiment 3. Time-dependent force-field's period was fixed to 0.7 seconds. Experiment 3 consisted of two sub-experiments. In the first sub-experiment, subjects were instructed to draw the reference circle for 150 laps at period 0.7 seconds. The period of drawing the circle and the force-field were the same. In another sub-experiment, they drew the reference circle for 150 laps at period 0.6 seconds in the second sub-experiment. In this case the two periods are different. The reference circle's band color information, combo information, catch trial distribution, and the fact that each sub-experiment consists of three phases are the same with Experiment 2.

5.4 Catch trial

5.4.1 Traditional catch trial for line movement

Catch trial is a popular technique to measure the degree of the trial-to-trial adaptation during an experiment. The traditional catch trial in line movement consists of a narrow tunnel-like error clamp model as shown in Figure 5.4. Assuming y-directional motion in linear motion, the channel force equation is expressed as

$$\vec{f_c} = \begin{pmatrix} -K & 0 \\ 0 & -K \end{pmatrix} \begin{pmatrix} x - x_d \\ 0 \end{pmatrix} + \begin{pmatrix} -B & 0 \\ 0 & -B \end{pmatrix} \begin{pmatrix} \dot{x} \\ 0 \end{pmatrix}. \tag{5.4.6}$$

which only applies the x-axis force, where x_d is the fixed value of starting point's x-coordinate. K was a spring stiffness and B was a damping coefficient.

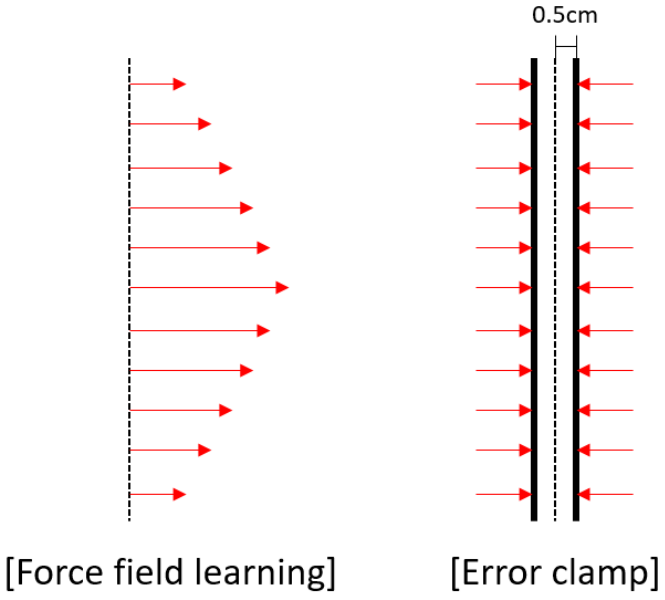

Figure 5.4: Learned force field and error clamp of line movement in catch trial.

5.4.2 New catch trial developed for continuous circular movement

In this study, a trial means drawing a circle in a circle, so we designed new catch trial appropriate for the circular movement. As you saw in the designed experiment above, each trial in the experiment was proceeded continuously without intermediate term. In order to test the trial-to-trial learning progress, the force-field is smoothly and unexpectedly changed to that of the catch trial in pseudo-random manner. The subjects are not noticed by the timing and even the existence of the catch trials. The force-field of catch trial for our study is designed as follows:

$$\vec{f_c} = \begin{pmatrix} -K & 0 \\ 0 & -K \end{pmatrix} \begin{pmatrix} x - x_d \\ y - y_d \end{pmatrix} + \begin{pmatrix} -B & 0 \\ 0 & -B \end{pmatrix} \begin{pmatrix} \dot{x} \\ \dot{y} \end{pmatrix}. \tag{5.4.7}$$

Equation 5.4.7 represented such a stiff spring-damper system. (x, y) meant the exact hand position, and $(\dot{x}, \dot{y})$ meant the exact hand velocity. (x_d, y_d) meant the point on the reference circle closest to (x, y). In other words, x_d and y_d were set as follows:

$$\begin{pmatrix} x_d \\ y_d \end{pmatrix} = \begin{pmatrix} R\cos\theta \\ R\sin\theta \end{pmatrix} = \begin{pmatrix} R\cos(\mathrm{atan2}(y, x)) \\ R\sin(\mathrm{atan2}(y, x)) \end{pmatrix} \tag{5.4.8}$$

where R is the rotation radius 7cm. K was a spring stiffness and B was a damping coefficient, and we fixed the gain parameters as $K = 8\mathrm{kN/m}$ and $B = 20\mathrm{Ns/m}$. The damping coefficient is properly tuned to prevent the hand from chattering problem caused by high stiffness. Such high stiffness is desirable since it restricts the hand to follow the reference circle trajectory precisely. During the catch trial, the forces that the subjects exerted in the direction perpendicular to the reference trajectory are recorded in the rate of 1kHz. The measured force trajectory indicates the prediction of the force-field by the internal model. The newly designed error clamp model is shown in Figure 5.5. Although the force of the channel trial

is determined, it is necessary to perform smooth transition in continuous operation. We defined a variable α to give a smooth transition to the channel trial by giving the following force:

$$\vec{f} = \alpha \vec{f_c} + (1 - \alpha)\vec{f_e} \tag{5.4.9}$$

where α is a function for a rotated angle θ that smoothly increases from 0 to 1 on the first rotation, constant from 1 to 1 on the second rotation, and smoothly decrements from 1 to 0 on the third rotation. The catch trial uses only data from the second rotation. It may seem inefficient because it ignores one rotation back and forth, but it was not significantly affected by the actual performance. Since the catch trial transits naturally, we can get better channel effect during experiment.

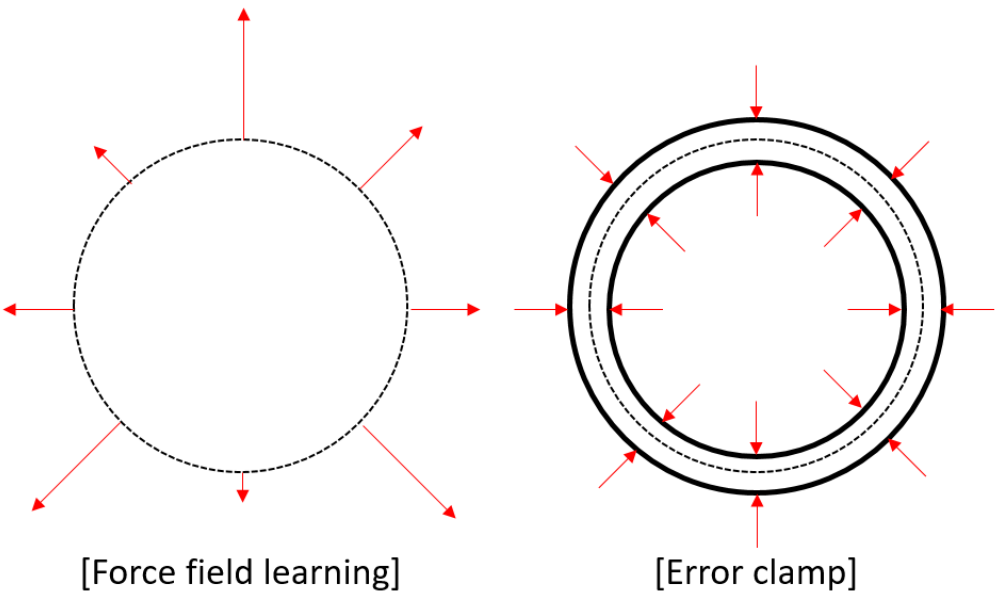

Figure 5.5: Learned force field and error clamp of circular movement in catch trial.

6

Conclusion

We introduce a new concept of the encoding capacity, which describes how much a force-field information the internal model can hold. We conduct some well-defined experiments to observe how learning patterns change with the size of the encoding space and the difficulty of the force field. As a result, we confirmed that the better the encoding capacity, the better the motor learning through newly designed catch trial. In learning curve based on position error, learning effect and signal-dependent effect were combined, then we analyzed this phenomenon more quantitatively using the complexity of the force-field. Simulation results based on the computational model explains the experimental results well. From now on, there are many cases where motivation is obtained from human motor control and applied to robot. The cases where human motor control research helps people rehabilitate also exist. Signal dependent noise exists in both humans and robots, and it is very important to consider this concept when learning internal model correspond to changed dynamics. Therefore, we think further research related to interaction between learning and signal dependent noise should be needed.

Bibliography

[1] Reza Shadmehr and Ferdinando A Mussa-Ivaldi. Adaptive representation of dynamics during learning of a motor task. *Journal of Neuroscience*, 14(5):3208–3224, 1994.

[2] Amir Karniel and Ferdinando A Mussa-Ivaldi. Sequence, time, or state representation: how does the motor control system adapt to variable environments? *Biological cybernetics*, 89(1):10–21, 2003.

[3] Michael A Conditt and Ferdinando A Mussa-Ivaldi. Central representation of time during motor learning. *Proceedings of the National Academy of Sciences*, 96(20):11625–11630, 1999.

[4] Eun Jung Hwang, Maurice A Smith, and Reza Shadmehr. Adaptation and generalization in acceleration-dependent force fields. *Experimental brain research*, 169(4):496, 2006.

[5] Kurt A Thoroughman and Reza Shadmehr. Learning of action through adaptive combination of motor primitives. *Nature*, 407(6805):742, 2000.

[6] Opher Donchin, Joseph T Francis, and Reza Shadmehr. Quantifying generalization from trial-by-trial behavior of adaptive systems that learn with basis functions: theory and experiments in human motor control. *Journal of Neuroscience*, 23(27):9032–9045, 2003.

[7] Luis Nicolas Gonzalez Castro, Craig Bryant Monsen, and Maurice A Smith. The binding of learning to action in motor adaptation. *PLoS computational biology*, 7(6):e1002052, 2011.

[8] Wilsaan M Joiner, Obafunso Ajayi, Gary C Sing, and Maurice A Smith. Linear hypergeneralization of learned dynamics across movement speeds reveals anisotropic, gain-encoding primitives for motor adaptation. *Journal of neurophysiology*, 105(1):45–59, 2010.

[9] Eun Jung Hwang, Opher Donchin, Maurice A Smith, and Reza Shadmehr. A gain-field encoding of limb position and velocity in the internal model of arm dynamics. *PLoS biology*, 1(2):e25, 2003.

[10] Eun Jung Hwang and Reza Shadmehr. Internal models of limb dynamics and the encoding of limb state. *Journal of neural engineering*, 2(3):S266, 2005.

[11] Gary C Sing, Wilsaan M Joiner, Thrishantha Nanayakkara, Jordan B Brayanov, and Maurice A Smith. Primitives for motor adaptation reflect correlated neural tuning to position and velocity. *Neuron*, 64(4):575–589, 2009.

[12] Jordan B Brayanov, Daniel Z Press, and Maurice A Smith. Motor memory is encoded as a gain-field combination of intrinsic and extrinsic action representations. *Journal of Neuroscience*, 32(43):14951–14965, 2012.

[13] Gary C Sing, Simon P Orozco, and Maurice A Smith. Limb motion dictates how motor learning arises from arbitrary environmental dynamics. *Journal of neurophysiology*, 109(10):2466–2482, 2013.

[14] Ken Takiyama, Masaya Hirashima, and Daichi Nozaki. Prospective errors determine motor learning. *Nature communications*, 6:5925, 2015.

[15] James N Ingram, Mohsen Sadeghi, J Randall Flanagan, and Daniel M Wolpert. An error-tuned model for sensorimotor learning. *PLoS computational biology*, 13(12):e1005883, 2017.

[16] Se-Woong Park, Hamal Marino, Steven K Charles, Dagmar Sternad, and Neville Hogan. Moving slowly is hard for humans: limitations of dynamic primitives. *Journal of neurophysiology*, 118(1):69–83, 2017.

[17] Christopher M Harris and Daniel M Wolpert. Signal-dependent noise determines motor planning. *Nature*, 394(6695):780, 1998.

[18] Kelvin E Jones, Antonia F de C Hamilton, and Daniel M Wolpert. Sources of signal-dependent noise during isometric force production. *Journal of neurophysiology*, 88(3):1533–1544, 2002.

[19] Paul M Fitts. The information capacity of the human motor system in controlling the amplitude of movement. *Journal of experimental psychology*, 47(6):381, 1954.

[20] Francesco Lacquaniti, Carlo Terzuolo, and Paolo Viviani. The law relating the kinematic and figural aspects of drawing movements. *Acta psychologica*, 54(1-3):115–130, 1983.

[21] Neville Hogan. An organizing principle for a class of voluntary movements. *Journal of Neuroscience*, 4(11):2745–2754, 1984.

[22] Yoji Uno, Mitsuo Kawato, and Rika Suzuki. Formation and control of optimal trajectory in human multijoint arm movement. *Biological cybernetics*, 61(2):89–101, 1989.

[23] Emanuel Todorov and Michael I Jordan. Optimal feedback control as a theory of motor coordination. *Nature neuroscience*, 5(11):1226, 2002.

[24] Emanuel Todorov and Michael I Jordan. A minimal intervention principle for coordinated movement. In *Advances in neural information processing systems*, pages 27–34, 2003.

[25] Ian S Howard, James N Ingram, and Daniel M Wolpert. Separate representations of dynamics in rhythmic and discrete movements: evidence from motor learning. *Journal of Neurophysiology*, 105(4):1722–1731, 2011.

[26] Ian S Howard, James N Ingram, and Daniel M Wolpert. A modular planar robotic manipulandum with end-point torque control. *Journal of neuroscience methods*, 181(2):199–211, 2009.

국문초록

가변 환경에 대한 인간 동역학의 적응은 인터널 모델의 개념으로 잘 설명된다. 인터널 모델은 일반적으로 운동 피질 뉴런에서 영감을 얻은 동적 원소들의 가중치 조합으로 매개 변수화된다. 동적 원소에 대한 다양한 표현이 존재하며 각 모델은 사람의 동역학 적응의 특성을 설명하는 데 성공했다. 그러나 인터널 모델이나 동적 원소를 통한 적응의 한계는 많이 연구되지 않았다. 더불어, 인터널 모델 학습을 연구할 때 신호 의존 노이즈를 고려하는 것이 중요함에도 불구하고, 그것에 대한 연구는 거의 진행되지 않았다. 이 논문에서 우리는 다음의 가설을 검증하고자 하였다: "인코딩 공간이 클수록 학습 효과가 더 좋다." 위치 오류 수준에서 우리는 외부 환경의 훈련 양과 신호 의존 노이즈이 어떻게 상호 작용을 하는지 외부 힘장 복잡성의 조절을 통해 조사했다. 특히 우리는 연속적인 원 운동에서 새로운 캐치 트라이얼을 개발하고 원 운동 중에 인간의 인터널 모델에 의해 추정 된 힘장을 정량적으로 측정했다. 위의 두 실험 결과는 제안된 가설을 검증 할 수 있는 충분한 증거가 되었다. 실험 결과와 가설을 검증하기 위해 동적 원소의 조합을 기반으로 한 시뮬레이션 연구도 제안되었다.

주요어: 인간 동작 제어, 동역학 적응, 인터널 모델, 상태 공간 표현식, 동적 원소, 신호 의존 노이즈, 인코딩 공간

학번: 2017-22513